INVESTIGATIONS OF QCD HADRONIZATION USING JETS MEASURED AT $\sqrt{s} = 8$ TeV WITH THE ALICE DETECTOR.

A Dissertation Presented for the

Doctor of Philosophy

Degree

The University of Tennessee, Knoxville

Andrew John Castro

March 2019

"Do you ever do something, and then think to yourself: That's So Raven?."

— Zach Galifinakis

Table of Contents

List of Tables

List of Figures

Chapter 1

The LHC and ALICE

1.1 Overview of the LHC

The Large Hadron Collider(LHC)[30] is a circular particle accelerator located on the Franco-Swiss border near the city of Geneva. It is operated by the European Organization for Nuclear Research(CERN) and has carried out proton-proton(pp), lead-proton(pPb), and lead-lead(PbPb) collisions at center of mass energies of 0.9-14 TeV, 5.0 TeV, and 2.76-5.5 TeV respectively. The LHC is approximately 17 miles in circumference and located 200 meters underground. It is located inside the old accelerator tunnel used by the Large Electron-Positron[33] collider of the 1980's. There are over 8000 physicists and engineers making up the four main experiments at the LHC: ATLAS[1], CMS[18], LHCb[12], and ALICE[3]. Numerous physics results have been published with the most famous being the discovery of the Higgs boson in 2012[19][2].

Figure 1.1 shows a schematic of the LHC along with the pre-accelerators that help to accelerate protons and ions to their final energies before a collision at one of the four experimental interaction points(IP). Protons are injected into the LHC together in groups called 'bunches'. Every bunch is comprised of about 120 billion protons with about 50 nanoseconds between the arrival of the next bunch. The bunch scheme during the heavy-ion run is reduced to 200 nanoseconds due to the high multiplicity of the events and additional computational resources needed.

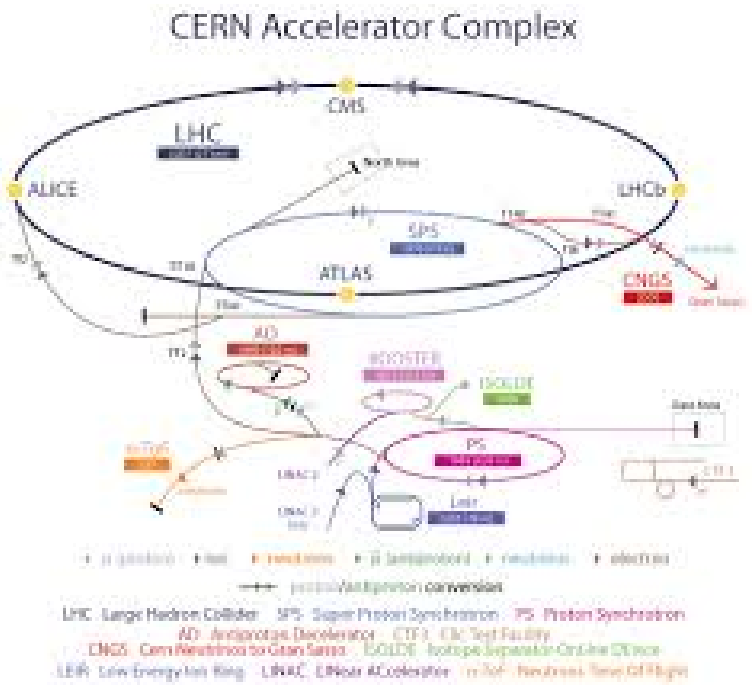

Figure 1.1: LHC accelerator complex. The four main experiments are shown in their relative locations[29].

1.1.1 LHC Operations

The LHC first attempted particle collisions in September of 2008. The initial ramping up of the super conducting magnets lead to mechanical failure of the helium pipes inside of the LHC beam line. This fault caused the LHC to remain shut down for over a year while the accelerator was repaired and new safety procedures were implemented. The first successful collisions occurred in 2009 with proton collisions at a reduced energy of 0.9 TeV. 2010 marked the beginning of a new era in high energy frontier with proton collisions at a record setting 7 TeV. The only other major fault that has occurred was in the summer of 2016. A stone marten chewed through a high voltage line in a power transformer on a ground level building at the LHC. The LHC went offline for about a week while repairs occurred and quickly resumed the physics program. Unfortunately, the marten did not survive.

The typical operating year at the LHC allows for any repairs or upgrades on any of the experiments to be performed during the offline period for the first 3 months. After the offline period the proton physics program begins and lasts until approximately mid-November. From mid-November until mid-December is the heavy-ion program at CERN,

which is when either PbPb or pPb collisions occur. After mid-December the LHC shuts down for the remainder of the year. From 2014 until mid-2015 the LHC was shutdown for major renovations and upgrades for the LHC accelerator and a number of sub-detectors on each experiment, this was known as long shutdown 1(LS1). After 2018, the LHC will go through another shutdown (LS2) during which the accelerator will have a high luminosity(Hi-Lumi) upgrade. This will be discussed in detail along with the upgrades that will be done to ALICE in chapter **??**.

1.1.2 LHC Accelerator Complex

The LHC accelerator complex is a succession of particle accelerators that increase the energy of particles before they are injected into the next accelerator. Hydrogen atoms are first passed through a high voltage environment that strip any electrons around the nuclei. Once the nuclei are stripped of their electrons they are injected into the linear accelerator(LINAC). The LINAC uses radio frequency cavities to accelerate particles to 50 MeV before they enter the first circular accelerator the Proton Synchrotron(PS). The PS begins to focus the protons into bunches and further accelerates them to 1.4 GeV before the the beam enters the Super Proton Synchrotron(SPS). The SPS will further separate the bunches in the beam to the predetermined beam parameters and accelerate the particles to 450 GeV. The beam is then injected into the LHC. Once the beams are injected into the LHC they are accelerated to the final collision energy. Afterwards the beams get 'squeezed', or tightly focused. The final step is to 'adjust' to the beams to overlap with one another at each experiments IP. This entire process from stripping the electrons to having collisions in each IP takes 20 minutes.

In order for the beam parameters to be maintained in the LHC, numerous dipole and quadrupole magnets are deployed to accelerate, focus, and bend the particle beams. The magnets use a superconducting niobium-titanium alloy that are maintained at an operating temperature of 1.9 K using helium-4. Upgrading these magnets is one of the major goals during LS2 as part of the Hi-Lumi upgrade of the LHC[21].

1.2 The ALICE Experiment

A Large Ion Collider Experiment(ALICE) is a general purpose detector that covers a solid angle of 4π around the IP at point 2 of the LHC. It is 26 m long, 16 m high, 16 m wide, and weighs approximately 10,000 tons[21]. Like many other large scale detectors ALICE is made up of a number of sub-detectors[1] that perform tracking, particle identification(PID), timing, vertex reconstruction, and calorimetry.

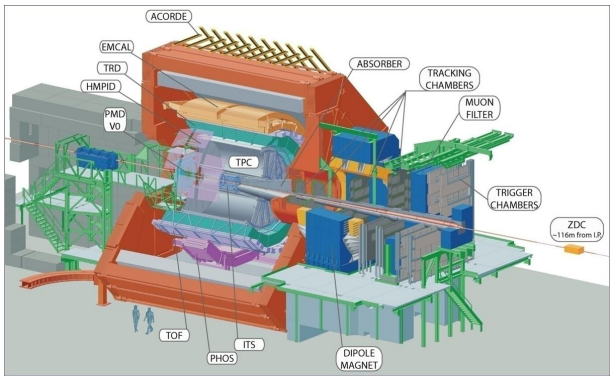

Figure 1.2: The ALICE Detector[10].

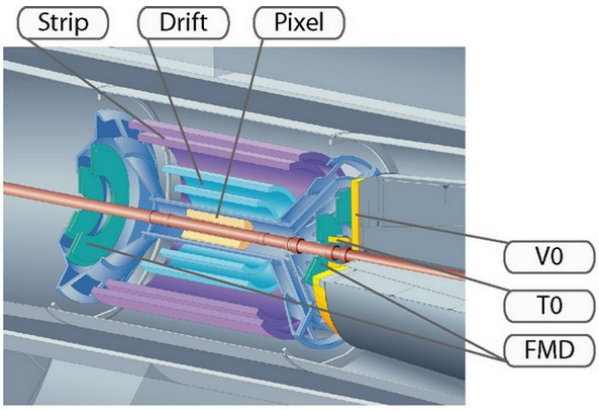

Figure 1.3: ALICE Inner tracker, timing, and vertex detectors located near interaction point[10].

Figure 1.2 shows the ALICE detector with human figures to set the scale. Figure 1.3 shows the area closest to the IP with the TZERO, VZERO, Inner Tracking System and Forward Multiplicity Detector; these detectors give basic information on the collison such as vertex location, centrality, timing, etc. Further out from the central region are a number of

[1] In total ALICE has 18 sub-detectors

tracking detectors like the Time Projection Chamber and Time-of-Flight detectors that focus on measuring charged particle momentum and PID. Next are the calorimeters that measure particle and jet energies, such as the Electromagnetic Calorimeter, Photon Spectrometer, and the Dijet Calorimeter. All of these sub-detectors housed in the L3 magnet seen as the red octagon in Figure 1.2. The L3 magnet provides a uniform magnetic field over the central area of ALICE and is responsible for the high PID performance ALICE has over a wide kinematic region[24]. At high psuedorapidity their is a muon tracker and trigger for muon physics. The following sections will give a more detailed discussion of the sub-detectors used for this analysis

1.2.1 TZERO

The TZERO(T0)[14] detector is a double layer Cherenkov counter located at 70 cm(T0A) and 370 cm(T0B) from the IP. T0 functions as a trigger and timing detector that determines the precise moment in time at which an event 'starts' in the ALICE detector. The timing information from the T0 is fed to other sub-detectors, like the Time-of-Flight and Time Projection Chamber detector, for track reconstruction. The T0 also gives feedback on the target luminosity of the ALICE experiment to the LHC operations center.

1.2.2 VZERO

The VZERO(V0)[4] detector is a double layer scintillator array and similar to the T0 is asymmetrically placed at a distance of 86 cm(V0A) and 329 cm(V0C) away from the primary IP. It provides the 'minimum bias'(MinBias)[2] trigger information for events and centrality information during the heavy-ion run. Centrality is determined by measuring the multiplicity amplitude from the V0 and fitting these results to a Glauber[3] distribution, as seen in Figure 1.4. The V0 is also capable of precision measurements of the target luminosity in the ALICE detector.

[2] A MinBias event is unsurprisingly defined as an event with the least amount of bias possible. Events recorded with a MinBias trigger attempt to not artificially prefer either diffractive or non-diffractive processes over one another[23].

[3] A Glauber model treats the nucleons composing a nucleus as hard shells, more can be found here [28].

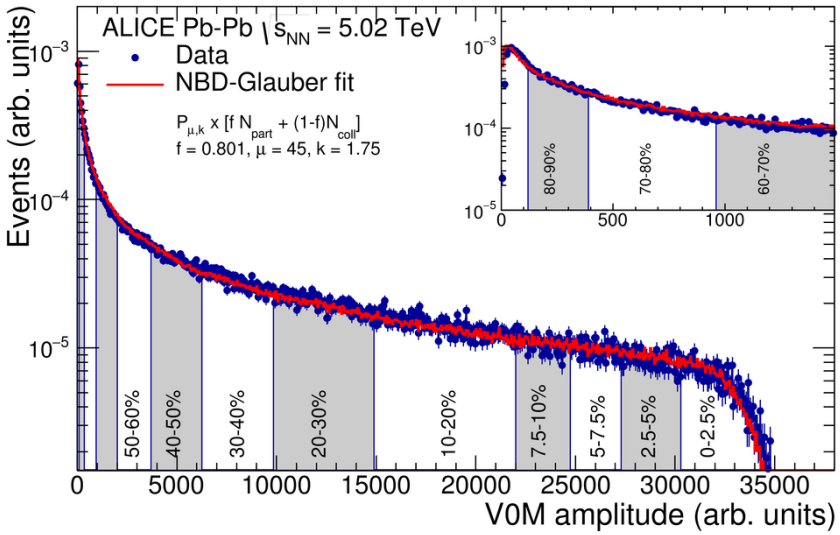

Figure 1.4: Multiplicity measured in the V0 detector with Glauber fits corresponding to centrality[8].

1.2.3 Inner Tracking System

The Inner Tracking System(ITS)[13] is a six layers solid state silicon detectors. Closest to the beam line are two layers of Silicon Pixel Detectors, the next two layers are Silicon Drift Detectors, and furthest from the beam line are two layers of Silicon Strip Detectors. The main purpose of the ITS is to perform momentum measurements, PID, and vertex reconstruction of charged tracks. PID[4] is performed by measuring the ionization energy, $\frac{dE}{dx}$, of charged particles as they traverse the detector[9]. The ITS has a spatial resolution of 100 μm, this allows for measurements of short lived hadrons by reconstructing secondary vertices.

1.2.4 Time Projection Chamber

The Time Projection Chamber(TPC)[11] is a gaseous charged particle tracker and the largest of its kind in the world. The TPC has full azimuthal coverage, a pseudorapidity acceptance of $|\eta| \leq 0.7$, and a volume of 93 m^2. Figure 1.5 shows a schematic of the TPC. As charged particles traverse the drift volume of the TPC, they ionize the gas inside[5]. A central cathode in the TPC wth a voltage of 100 kV induces a uniform electric field of 400 V/m along the

[4]see appendix A

[5]The TPC has operated with Ne – CO_2 (90-10) and Ar – CO_2 (90-10) gas mixtures in the past

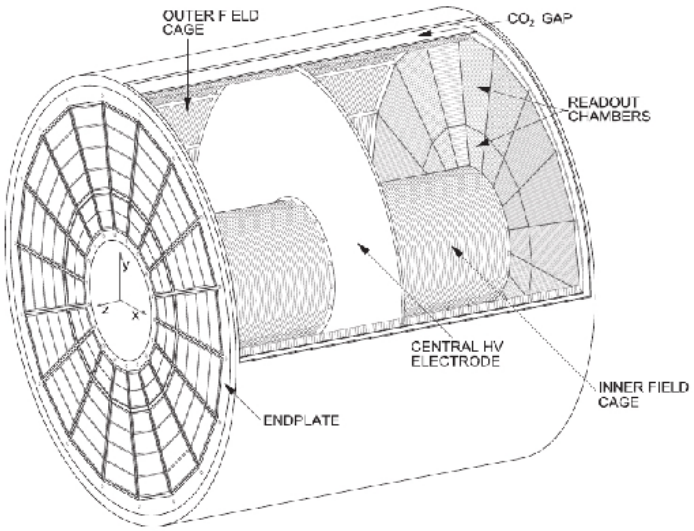

Figure 1.5: The ALICE Time Projection Chamber[11].

beam axis throughout the drift volume. Ionized electrons will drift down to the cylindrical endcaps of the TPC where the read-out chambers(ROC) are located. There are 18 ROCs on each side of the TPC which are further broken into a Inner Read Out Chamber(IROC) and Outer Read Out Chamber(OROC).

The TPC readout

The TPC incorporates a Multi-Wire Proportional Chamber(MWPC) design for amplification and copper pads for readout[6]. Ionized electrons created from charged particles take approximately 100 μs to move from the drift volume to the readout region. Once these electrons enter the readout region they will undergo an amplification process with the MWPC, seen as the sensing grid wires in Figure 1.6. This amplification process will turn the few dozen ionization electrons generated from a charged particle into thousands of amplification electrons that are easily sensed by the cooper pads and read from the front-end electronics(FEE). Amplification using MWPCs has the disadvantage of creating thousands of ions known as 'backflow ions' that can move back into the drift volume of the TPC. The presence of backflow ions in the drift volume of the TPC will cause distortions in the uniform electric field of the TPC. These distortions are known as 'space-charge' distortions

[6]Their are 72 MWPCs and 500K copper pads in the ALICE TPC

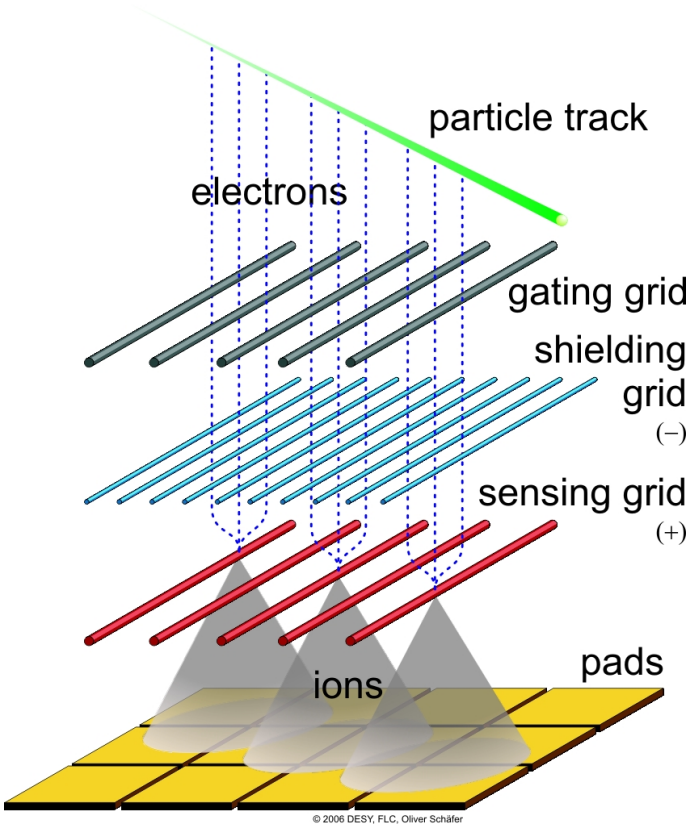

Figure 1.6: The TPC readout region[Diener].

and will compromise the physics performance of the TPC. In order to minimize the space-charge distortions the TPC incorporates a gating grid[**?**]. Once an event is detected in the readout electronics of the TPC a high voltage is induced on the gating grid. This will capture any backflow ions moving from the amplification region to the drift volume. When engaged the gating grid introduces a dead time as any ionization electrons from new events occurring in ALICE will also get captured. The current configuration of the gating grid is designed to engage it for 300 μs after an event is first detected. This has been shown to absorb approximately 99% of the backflow ions created while preserving the TPC physics performance. The deadtime due to the gating grid along with the drift time for charged particles in the TPC limits the readout to 3.5 kHz. Upgrading the triggered operation of the current TPC to a continuous readout for the Hi-Lumi upgrade of the LHC will be discussed in detail in Chapter **??**.

TPC Performance

In order to reconstruct the trajectory of a particle, an iterative process known as the Kalman filter approach is deployed. The x-y coordinate which is perpendicular to the beamline are determined via the signal induced on the copper pads. The z component which is parallel to the beamline is reconstructed using the timing information from the T0.

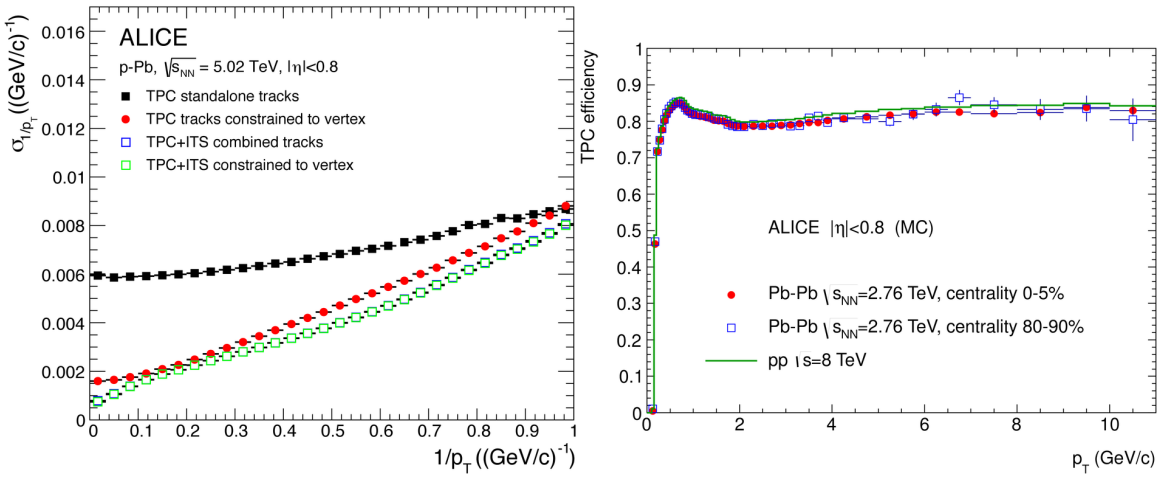

(a) TPC momentum resolution **(b)** ITS-TPC track matching efficiency

Figure 1.7: TPC momentum and tracking resolution[5].

The TPC has excellent momentum resolution between 150 MeV/c to 100 GeV/c[27]. Figure 1.7a shows the inverse momentum resolution as being below 10% in black. The momentum resolution was further improved to almost 5% over the full kinematic range by matching TPC tracks to ITS tracks and constraining those tracks to orignating from the primary vertex region, red and green respectively. The matching efficency between ITS tracks to TPC tracks is stable at about 80%, Figure 1.7b.

1.2.5 Electromagnetic Calorimeter

The Electromagnetic Calorimeter(EMCal)[22] is a lead based sampling calorimeter located at a radius of 4.5 meters from the beam pipe. It covers a pseudorapidity of $|\eta| \leq 0.7$ and has azimuthal coverage of $\Delta\phi = 107\,\text{deg}$.

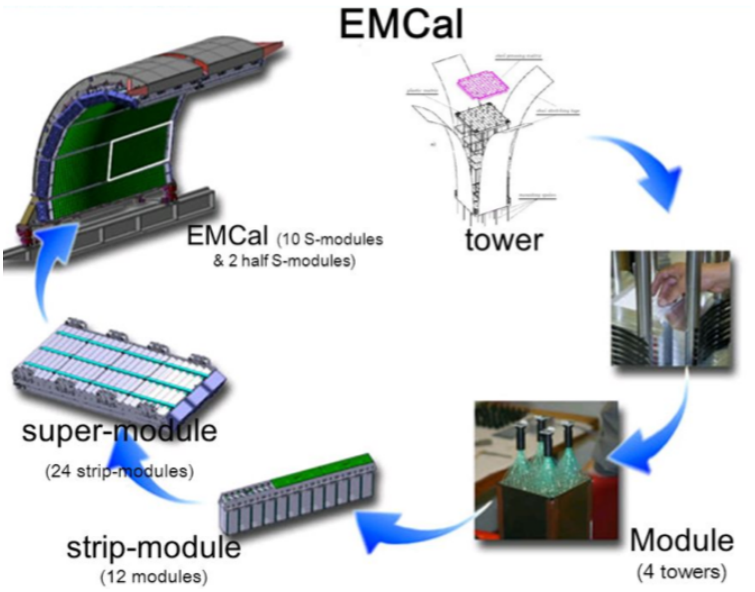

Figure 1.8: ALICE EMCal along with super modules, tower strips, and towers[15].

Figure 1.8 shows the layout of the EMCal. The smallest element of the EMCal is the 'tower'[7]. The tower serves as the readout and is made up of several layers of alternating scintillator and Pb-absorber. Particles that interact via the electromagnetic force initiate a shower in the absorber material in the tower. This electromagnetic shower induces light in the scintillator to accumulate in the avalanche photodiodes(APD) in proportion to the particle's energy. A 'module' is an array of four towers that share readout electronics. Twelve modules will be placed in a single strip that provides support to the structure. The largest component of the EMCal is the super-module, consisting of 1,100 towers, which serves as the mounting structure to the ALICE detector. In 2015 Dijet Calorimeter(DCAL) was installed in the ALICE detector to perform back-to-back jet measurements.

EMCal Performance

As particles enter the EMCal they initiate an electromagnetic shower. The shower of electromagnetic particles spans several neighboring towers, these towers are grouped together into 'clusters' and the Analog-To-Digital Conversion(ADC) signal from the clusters corresponds to the energy deposited by the particle. The EMCal was designed so that photons and electrons will fully shower inside of the tower region and thus fully deposit their

[7]There are 12K towers in the EMCal

energy. Hadrons on the other hand will punch through the EMCal and only deposit a small fraction of their energy. PID can be performed using the EMCal via track-cluster matching from the TPC. TPC tracks are geometrically matched to the centroid of a cluster and if no track is matched the cluster originated from a photon. If a track is matched, then the ratio of E/P, the energy of a matched cluster to the momentum of a TPC track, can be used to separate electrons from hadrons.

The energy resolution of the EMCal follows the form seen in equation 1.1

$$\frac{\sigma}{\mathrm{E}} = \sqrt{\mathrm{A}^2 + \frac{\mathrm{B}^2}{\mathrm{E}} + \frac{\mathrm{C}^2}{\mathrm{E}^2}} \tag{1.1}$$

where E is the cluster energy, A characterizes stochastic fluctuations such as photon collection efficency, B is a function of the systematic effects such as detector non-uniformity, and C is a function of the noise in the Front-end electronics.

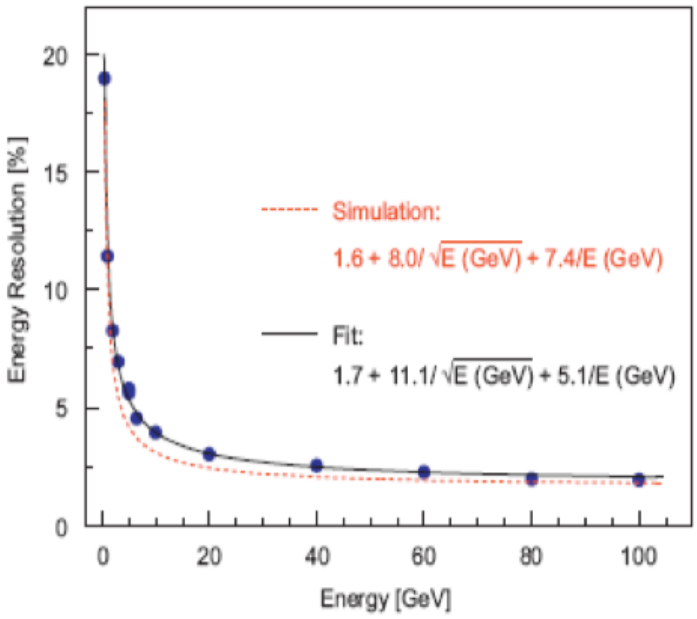

Figure 1.9: Energy resolution in the EMCal measured in a 2007 test beam at CERN(blue) compared to GEANT3 simulations of the EMCal(orange), fits for the parameters A, B, and C are also shown[7].

As seen in figure 1.1 excellent agreement exits between the measured performance of the EMCal compared to simulations in a kinematic range between 10GeV – 100GeV. The stochiastic term, A, is the largest source of uncertainty in the energy resolution due to the

EMCal being a sampling calorimeter. Unlike the TPC the resolution improves at high-p_t making the EMCal ideal for measuring high energy particles and jets

EMCal Trigger

Due to the high luminosity in the LHC only a small fraction of events may be recorded to disk for later analysis. ALICE employs a variety of triggers to record events that have the highest value for performing quality physics analysis. The EMCal can trigger on events in order to increase the effective sample size for high-p_T jets, photons, and electrons. The two main triggers[17][16] for the EMCal are a jet trigger and a gamma trigger. The gamma trigger is comprised of a 4x4 patch of EMCal towers, while the jet trigger is a 16x16 patch of towers. Once the gamma trigger has surpassed a minimum energy threshold of 5 GeV[26] the event is tagged as a gamma event and the patch location is recorded.

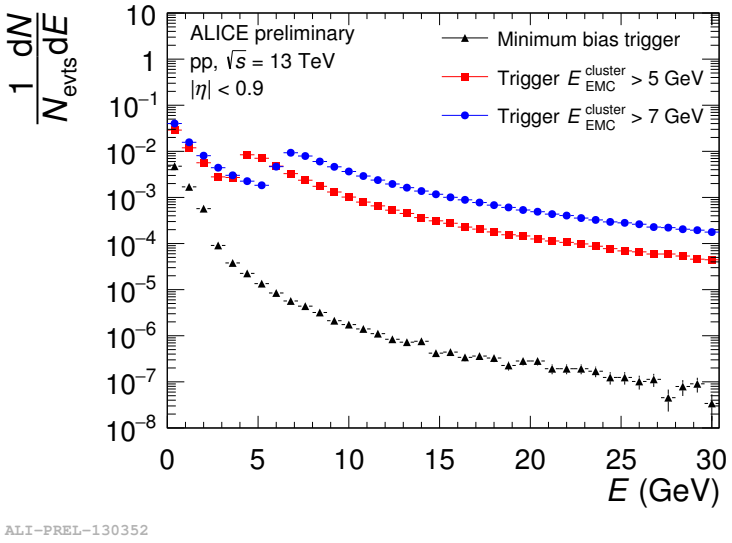

Figure 1.10: Cluster Spectra from the ALICE EMCal. MinBias is shown in black while the red and blue points show the spectra using the gamma trigger at two energy thresholds[25].

EMCal jet triggered events have an energy threshold of 20 GeV and are similarly tagged and recorded. Figure 1.10 shows the spectra from clusters measured in the EMCal using MinBias data in black and the gamma trigger from the EMCal set to two thresholds, 5 GeV and 7 GeV. Recording the events that satisfy the EMCal triggers introduces a bias towards high-p_T processes, however by using events that had an EMCal trigger we can extend the

kinematic range of an inclusive jet measurement as seen in Figure 1.10. In order to account for this bias it is necessary to calculate a trigger efficiency by comparing spectra from inclusive jets recorded using the MinBias trigger to the spectra generated from the EMCal triggers. The calculation of the trigger efficiency will be discussed in depth in section **??**

Bibliography

[1] Aad, G. et al. (2008). The ATLAS Experiment at the CERN Large Hadron Collider. *JINST*, 3:S08003. 1

[2] Aad, G. et al. (2012). Observation of a new particle in the search for the Standard Model Higgs boson with the ATLAS detector at the LHC. *Phys. Lett.*, B716:1–29. 1

[3] Aamodt, K. et al. (2008). The ALICE experiment at the CERN LHC. *JINST*, 3:S08002. 1

[4] Abbas, E. et al. (2013). Performance of the ALICE VZERO system. *JINST*, 8:P10016. 5

[5] Abelev, B. B. et al. (2014a). Performance of the ALICE Experiment at the CERN LHC. *Int. J. Mod. Phys.*, A29:1430044. vi, 9

[6] Abelev, B. B. et al. (2014b). Production of charged pions, kaons and protons at large transverse momenta in pp and Pb–Pb collisions at $\sqrt{s_{NN}}$ =2.76 TeV. *Phys. Lett.*, B736:196–207. 20

[7] Abeysekara, U. et al. (2010). ALICE EMCal Physics Performance Report. vi, 11

[8] Adam, J. et al. (2016a). Centrality dependence of the charged-particle multiplicity density at midrapidity in Pb-Pb collisions at $\sqrt{s_{NN}} = 5.02$ TeV. *Phys. Rev. Lett.*, 116(22):222302. vi, 6

[9] Adam, J. et al. (2016b). Particle identification in ALICE: a Bayesian approach. *Eur. Phys. J. Plus*, 131(5):168. 6

[10] Alberico, W. M., Beraudo, A., De Pace, A., Molinari, A., Monteno, M., Nardi, M., and Prino, F. (2011). Heavy-flavour spectra in high energy nucleus-nucleus collisions. *Eur. Phys. J.*, C71:1666. vi, 4

[11] Alme, J. et al. (2010). The ALICE TPC, a large 3-dimensional tracking device with fast readout for ultra-high multiplicity events. *Nuclear Instruments and Methods in Physics Research A*, 622:316–367. vi, 6, 7

[12] Alves, Jr., A. A. et al. (2008). The LHCb Detector at the LHC. *JINST*, 3:S08005. 1

[13] Beolè, S. (2012). The alice inner tracking system: Performance with proton and lead beams. *Physics Procedia*, 37:1062 – 1069. Proceedings of the 2nd International Conference on Technology and Instrumentation in Particle Physics (TIPP 2011). 6

[14] Bondila, M. et al. (2005). ALICE T0 detector. *IEEE Trans. Nucl. Sci.*, 52:1705–1711. 5

[15] Bourdaud, G. (2008). Gamma-jet physics with the electro-magnetic calorimeter in the alice experiment at lhc. *Journal of Physics: Conference Series*, 110(3):032006. vi, 10

[16] Bourrion, O., Arbor, N., Conesa-Balbastre, G., Furget, C., Guernane, R., and Marcotte, G. (2013). The alice emcal l1 trigger first year of operation experience. *Journal of Instrumentation*, 8(01):C01013. 12

[17] Bourrion, O., Guernane, R., Boyer, B., Bouly, J., and Marcotte, G. (2010). Level-1 jet trigger hardware for the alice electromagnetic calorimeter at lhc. *Journal of Instrumentation*, 5(12):C12048. 12

[18] Chatrchyan, S. et al. (2008). The CMS Experiment at the CERN LHC. *JINST*, 3:S08004. 1

[19] Chatrchyan, S. et al. (2012). Observation of a new boson at a mass of 125 GeV with the CMS experiment at the LHC. *Phys. Lett.*, B716:30–61. 1

[Diener] Diener, R. Gas amplification with micro pattern gas detectors. vi, 8

[21] Fabjan, C. and Schukraft, J. (2011). The Story of ALICE: Building the dedicated heavy ion detector at LHC. In *'The Large Hadron Collider: A marvel technology', EPFL-Press Lausanne, Switzerland, 2009 (Editor: L. Evans), chapter 5.4.* 3, 4

[22] Fantoni, A. and the ALICE collaboration (2011). The alice electromagnetic calorimeter: Emcal. *Journal of Physics: Conference Series*, 293(1):012043. 9

[23] Field, R. (2011). Min-Bias and the Underlying Event at the LHC. *Acta Phys. Polon.*, B42:2631–2656. 5

[24] Gligorov, V. V., Knapen, S., Nachman, B., Papucci, M., and Robinson, D. J. (2018). Leveraging the ALICE/L3 cavern for long-lived exotics. 5

[25] Jahnke, C. (2018). J/ψ production as a function of event multiplicity in pp collisions at $\sqrt{s}$ = 13 TeV using EMCal-triggered events with ALICE at the LHC. In *14th International Workshop on Hadron Physics (Hadron Physics 2018) Florianopolis, Santa Catarina, Brazil, March 18-23, 2018*. vi, 12

[26] Kral, J., Awes, T., Muller, H., Rak, J., and Schambach, J. (2012). {L0} trigger for the {EMCal} detector of the {ALICE} experiment. *Nuclear Instruments and Methods in Physics Research Section A: Accelerators, Spectrometers, Detectors and Associated Equipment*, 693:261 – 267. 12

[27] Lippmann, C. (2012). Performance of the alice time projection chamber. *Physics Procedia*, 37:434 – 441. Proceedings of the 2nd International Conference on Technology and Instrumentation in Particle Physics (TIPP 2011). 9

[28] Loizides, C. (2016). Glauber modeling of high-energy nuclear collisions at the subnucleon level. *Phys. Rev.*, C94(2):024914. 5

[29] Mobs, E. (2016). The CERN accelerator complex. Complexe des accélérateurs du CERN. General Photo. vi, 2

[30] MYERS, S. (2013). The large hadron collider 2008–2013. *International Journal of Modern Physics A*, 28(25):1330035. 1

[31] Noferini, F. (2016). The ALICE PID performance in Run 1 and perspectives in view of Run 2. In *Proceedings, 3rd Large Hadron Collider Physics Conference (LHCP 2015): St. Petersburg, Russia, August 31-September 5, 2015*, pages 523–528, Gatchina. Kurchatov Institute, Kurchatov Institute. vi, 20

[32] Patrignani, C. et al. (2016). Review of Particle Physics. *Chin. Phys.*, C40(10):100001. vi, 19

[33] Taylor, T. and Treille, D. (2017). The Large Electron Positron Collider (LEP): Probing the Standard Model. *Adv. Ser. Direct. High Energy Phys.*, 27:217–261. 1

Appendices

A Particle Identification via Bethe-Bloch

The energy loss of a relativistic charged particle traversing through a medium is given by the Bethe-Bloch relation:

$$\frac{dE}{dx} \propto \frac{1}{\beta^2}\frac{Z}{A}\rho\left[\frac{1}{2}\ln\frac{2m_e c^2\beta^2\gamma^2 T_{max}}{I^2} - \beta^2 - \frac{\delta(\beta\gamma)}{2}\right] \tag{2}$$

where ρ is the density of the medium, $\frac{Z}{A}$ is the ratio of the atomic number to the atomic mass of the absorber, β is the ratio of the particle's momentum to energy, T_{max} is the maximum transfer energy from the charged particle to an electron in the medium, I^2 is the mean excitation energy of the medium, $\frac{\delta(\beta\gamma)}{2}$ is a correction factor based on the polarization of the material, and γ^2 is the lorentz factor $\frac{1}{\sqrt{1-\beta^2}}$

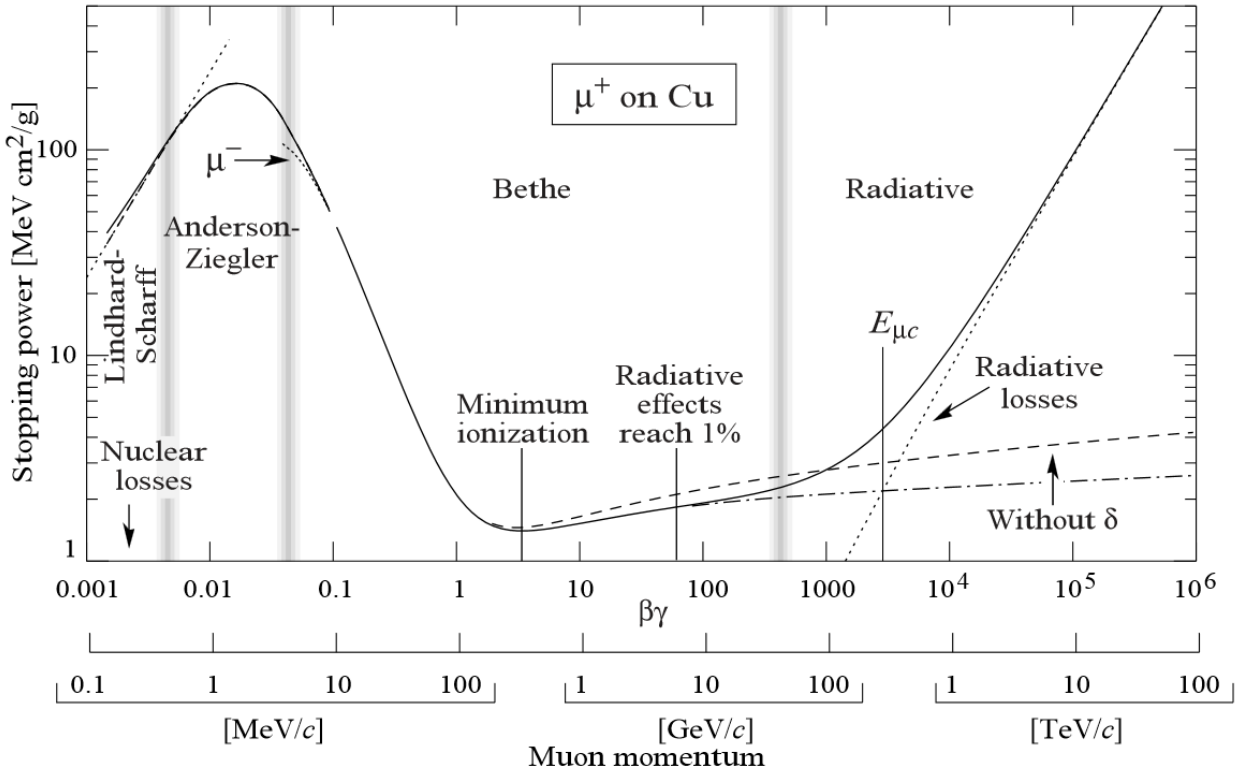

Figure 11: Energy loss of a muon traversing a copper medium between 0.1 MeV to 100 TeV [32].

Figure 11 shows the Bethe-Bloch curve for a muon over a wide kinematic range. At low energies the dominate form of energy loss is via elastic scattering, while at high energies

radiation becomes the dominate energy loss mechanism. When $\beta\gamma \approx 3$ the muon losses the least amount of energy possible and is called a minimum ionization particle(MIP).

The ALICE ITS and TPC[8] cannot directly measure the energy loss of a particle traversing either sub-detector. Instead they perform PID by measuring the relative amplitudes from the sub-detectors read-out elements, pixels in the ITS and copper pads in the TPC. The amplitudes are then fit to the Bethe-Bloch equation as seen in Figure 12. Electrons weakly obey the Bethe-Bloch relationship in the kinematic ranges sensitive to the ITS and TPC and thus have a constant energy loss in both detectors.

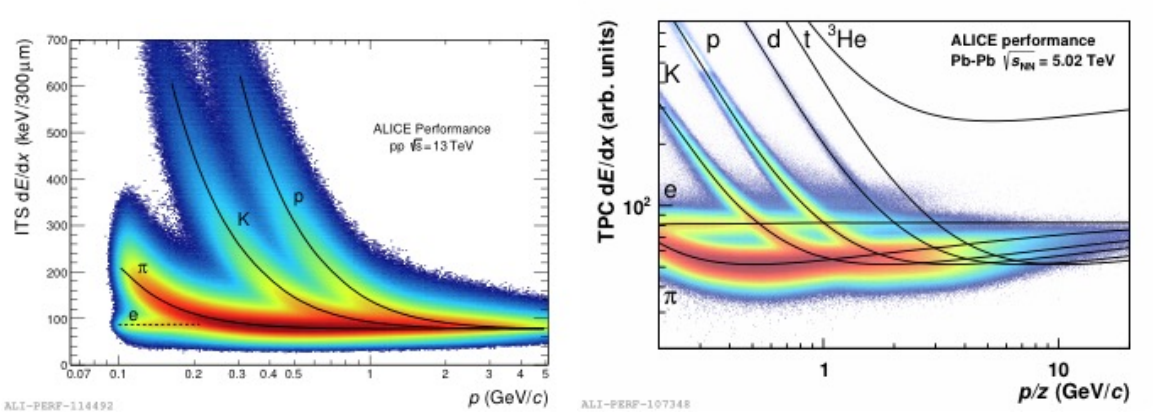

(a) ALICE ITS(pp $\sqrt{s} = 13$ TeV) **(b)** ALICE TPC (PbPb $\sqrt{s_{NN}} = 5.02$ TeV)

Figure 12: Specific energy loss for the ITS*(left)* and the TPC*(right)* with Bethe-Bloch fits from different particle species traversing each detector[31].

Figure 12 also shows that the Bethe-Bloch curves merge above some kinematic range, 4 GeV in the ITS and 10 GeV in the TPC. Above this kinematic range particles cannot be distinguished on a track-by-track basis, but by using statistical methods and Gaussian fits PID can be extended up to 20 GeV[6].

[8]See Section 1.2.3 and Section 1.2.4

Vita

Vita goes here. The vita should be a brief biography about the author written in third person and paragraph format. It should not be the author's resume or CV.